



Modeling of by-products from photocatalytic oxidation (PCO) indoor air purifiers: A case study of ethanol

Lexuan Zhong^{a,*}, Fariborz Haghighat^b

^a Department of Mechanical Engineering, University of Alberta, Edmonton, Alberta, T6G 1H9, Canada

^b Department of Building, Civil and Environmental Engineering, Concordia University, Montreal, Quebec, H3G 1M8, Canada



ARTICLE INFO

Keywords:

Photocatalytic oxidation (PCO)
By-products
Ethanol
Formaldehyde
Acetaldehyde
Modeling

ABSTRACT

Ultra-violet photocatalytic oxidation (UV-PCO) technology has been receiving extensive attention for indoor air purification in recent two decades. However, the formation of by-products during the UV-PCO process darken its prospect of providing healthy indoor air quality (IAQ). This study examines by-product generation and operational parameters from 36 UV-PCO tests using a pilot duct system with the objectives of developing reliable by-product predictive models. The statistical analysis aimed at establishing linear and non-linear regression models to predict the concentrations of formaldehyde and acetaldehyde based on factors such as concentration, RH, airflow, and irradiance. The developed linear models provided satisfactory estimations of acetaldehyde and the sum of formaldehyde and acetaldehyde (FA) levels with regression coefficients (R^2) of 0.74 and 0.84, respectively. Parametric study and bivariate analysis further confirm the statistical significance of independent variables on the acetaldehyde and FA productions. The PCO reaction pathway was proposed to explain that the presence of some strongly bounded intermediates on the surface decreased the reactivity of acetaldehyde to be further oxidized to formaldehyde.

1. Introduction

Heterogeneous ultra-violet photocatalytic oxidation (UV-PCO) based air cleaners have been receiving close attention recently due to its promising oxidation capability for a wide range of air pollutants, and thus it is capable of providing the sustainable indoor environment. An extensive body of research reports the performance of lab-scale UV-PCO air cleaners under various testing conditions and demonstrates their promising future of commercialization in a manner of stand-alone air cleaners or air cleaning units integrated into HVAC systems [1–8]. Different types of mathematical models, including analytical and numerical models, kinetic models, computational fluid dynamics (CFD) and empirical-based models, have been proposed to evaluate the UV-PCO removal efficiency of the tested compounds [9–17]. Although UV-PCO is an advanced technology for improving indoor air quality (IAQ), some researchers discovered that the operation of UV-PCO air cleaners might pose potential health risks due to the formation of carcinogenic compounds (e.g. formaldehyde, benzene) during air-cleaning processes [3,8,18–20]. Uncertain health exposure of PCO-based air cleaners in a building in terms of toxic by-product generation hinders immediate commercialization of PCO air purifiers and establishment of associated regulatory standards. In order to accelerate the progress of

commercialization, there is ample need for conducting more basic research work to eliminate these technological obstacles.

At present, most research on by-product generation still relies on experimental observation. For example, a list of by-products, such as formaldehyde, acetone, acetaldehyde, hexane, cyclohexane, benzene, crotonaldehyde, benzaldehyde, formic acid, benzoic acid, CO, CO₂, and so on, has been qualitatively and quantitatively identified in the literature under different environmental conditions with diverse challenge volatile organic compounds (VOCs) [3,8,18,19,21–25]. It was experimentally demonstrated that the challenge VOC type and concentration, ozone concentration, photocatalyst type, UV irradiance, airflow rate, as well as water vapor have impacts on the formation of by-products. Hence, the by-product generation is closely related to the PCO chemo-dynamic affected by each operational condition. However, there is limited research aiming to examine the relationship between by-products and operational parameters in a modeling manner, which is increasingly recognized as an essential methodological basis to obtain fundamental knowledge on health exposure of PCO-based air cleaners. Although some researchers proposed potential pathways [18,21,23] and empirical models [26–28] to describe the mechanism of specific by-product formation and kinetics, these models are site-specific due to the facts that kinetic values (e.g., adsorption coefficient, reaction constant)

* Corresponding author. 10-351 DICE, 9211-116 St NW, University of Alberta, Edmonton, Alberta, T6G 1H9, Canada.
E-mail address: lexuan.zhong@ualberta.ca (L. Zhong).

came from specific testing system setting-up, and their predictive capabilities could be limited under varying conditions. In addition, few attempts have been made to create statistical models for the prediction of by-product generation in the air treatment, which can be a useful tool to promote the standard/code development in the healthy building industry. Compared with discrete experimental data, statistical models provide an efficient strategy to deeply and completely explore both individual and interaction effects on by-product generation, which will help us find optimal conditions to minimize by-products.

For the first time, this paper presents the by-product predictive model development using the linear and nonlinear multi-regression technique with an emphasis on prediction of formaldehyde and acetaldehyde, two common gaseous by-products, under various experimental conditions in a pilot in-duct UV-PCO unit. A small PCO database was established to facilitate the by-product analysis. Effects of VOC concentration, RH, irradiance, airflow rate, and ozone parameters on by-product formation were statistically studied. Multiple linear and non-linear models were developed and validated for aldehyde prediction. The goodness of fit for the models was evaluated by the regression coefficient (R^2), Durbin-Watson value, Kolmogorov-Smirnov test, and ANOVA F-test. Validation results indicated that the predictive models could be used to forecast aldehyde generation in a wide range of UV-PCO applications. In addition, on the basis of observation and model simulation, the potential PCO reaction pathway of ethanol was proposed to explain why acetaldehyde, rather than formaldehyde, was a dominant by-product of PCO of ethanol.

2. Materials and methods

2.1. PCO-based air cleaner

The pilot test rig used in this study (Fig. 1) was an aluminum duct system with a cross-section area of $0.3 \text{ m} \times 0.3 \text{ m}$ ($1 \text{ ft} \times 1 \text{ ft}$). The duct was an open-loop mode system which was able to provide $135\text{--}270 \text{ m}^3/\text{h}$ ($80\text{--}160 \text{ cfm}$) airflow rates by a speed-controlled fan mounted at the end. A pleated fabric pre-filter was mounted at the beginning section of the test rig to remove potential particles in the introduced laboratory air. The air mixed with evaporated VOCs in the gas mixer chamber composed of a mixing baffle and a perforated plate so that the contaminated air was fed into the duct system with a uniform distribution. The upstream and downstream of the duct were fitted with perforated stainless steel cross tubes to collect inlet and outlet air samples by sampling pumps and a photoacoustic gas monitor. Sampling tubes were connected to the sampling pumps at a sampling rate of

$1.3 \text{ L}/\text{min}$ for 1.5 h to explore the generation of by-products. After the cross tubes, sensors were installed at the centre of the duct to continuously monitor airflow, RH and temperature at upstream and downstream, respectively. At the middle section of the duct, there were three PCO filters (Saint-Gobain, France) and totally 2–6 low-pressure mercury vapor lamps (Ster-L-Ray, Atlantic Ultraviolet Corp., USA) allocated in two banks. The PCO filters were composed of the fiberglass substrate with $4.6 \text{ wt}\%$ TiO_2 loading. Brunauer–Emmett–Tele (BET) surface area of PCO filters was $106 \text{ m}^2/\text{g}$, and average pore diameter was 3.6 nm . There was an approximate 5 cm distance between the surfaces of the UV lamps and the PCO filters. Two types of UV lamps (UVC and vacuum UV (VUV)) were employed to examine the impacts of ozone-assisted PCO on by-product generation. An online ozone analyzer was connected to the duct system through bulkhead unions on the side of the duct system for ozone measurements. The detailed description of the duct system with regard to test rig dimensions, PCO filter characterization, and contaminant generation system can be found in the previous studies [7,8].

2.2. Chemicals

HPLC grade ethanol (99.8%), TO11/IP-6A aldehyde/ketone-DNPH mixtures (analytical standard) for the HPLC calibration and anhydrous grade acetonitrile (99.8%) for the HPLC operation were obtained from the Sigma-Aldrich Corporation (Canada). Deionized water filtered with a Milli-Q system (MilliporeSigma, Canada) was used for the HPLC calibration.

2.3. Analytical methods

The duct air quality parameters including ethanol, formaldehyde, acetaldehyde, temperature, RH, airflow, irradiance, and ozone concentration were analyzed. The inlet and outlet concentrations of ethanol were detected by a calibrated online photoacoustic spectroscopy (PAS, INNOVA 1312, LumaSense Technologies, Inc., USA). An optical filter with a centre wavenumber of $9.4 \mu\text{m}$, which selectively measured the concentration of ethanol with the detection limit of 60 ppb , was installed in the PAS. The used optical filter was not affected by interference from carbon dioxide and water vapor and had no response for both formaldehyde and acetaldehyde. Analysis of formaldehyde and acetaldehyde in air was in compliance with the US Environmental Protection Agency Method TO11: aldehydes were trapped in a high purity silica adsorbent coated with 2, 4-dinitrophenylhydrazine (2, 4-DNPH) (Sigma-Aldrich Corp., USA) through

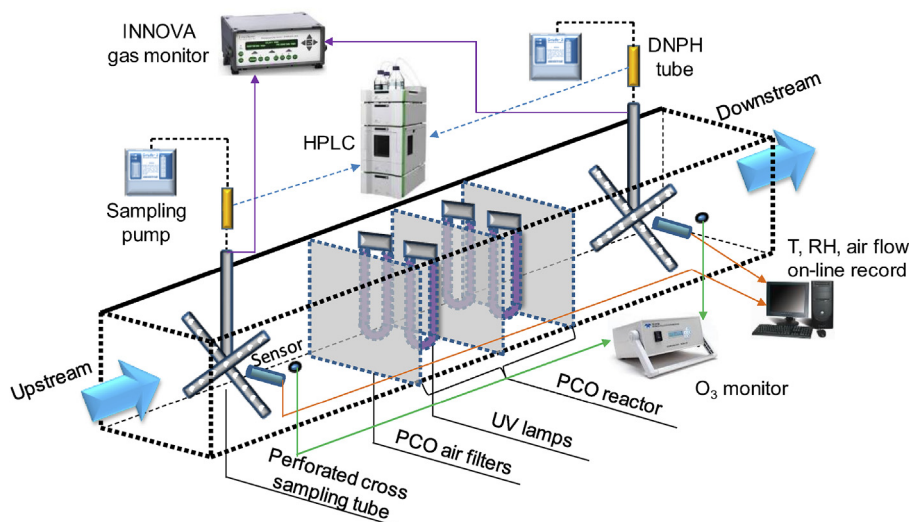


Fig. 1. Diagram of a UV-PCO duct system.

sampling pumps, followed by an offline High-Performance Liquid Chromatograph (HPLC, PerkinElmer, Inc., USA). The HPLC was equipped with a C18 Brownlee validated micro-bore column (150 mm × 4.6 mm ID, 5 μm film thickness) and a UV detector working at 360 nm. Acetonitrile and distilled water were used as the mobile phase with a flow rate of 1.0 mL/min. The detailed HPLC gradient analysis method includes: the ratio of 70% acetonitrile/30% water was held for 6 min, then the ratio increased to 100% acetonitrile/0% water and maintained for 3 min, and finally the ratio returned to 70% acetonitrile/30% water for 4 min.

The ozone concentration in effluent stream was measured by a calibrated ozone analyzer (Model 465L, Teledyne Technologies Inc, USA) using the technology of UV absorption. The analyzer was programmed to take samples continuously with the precision of ± 0.5% of full scale. The irradiance of 254 nm (UVC) and 185 nm (VUV) on the surface of the TiO₂ filter was monitored by a UV radiometer (Steril-Aire, Inc., USA) and a spectroradiometer (ILT900-R, International light Technologies, USA) respectively, with National Institute of Standards (NIST)-certified calibrations. The air conditions were monitored by a sensor (HMT 100, Vaisala, Finland) for humidity and temperature and an electronic low-flow probe (ELF-1200, EBTRON, USA) for airflow.

Potential formic and acetic acids from gaseous samples were analyzed by our collaborative lab in the department of Chemistry & Biochemistry. They used an HPLC system (Agilent, California, USA) with a Hi-Plex H column (7.7 × 300 mm, 8 μm, Agilent, USA) to separate acids. HPLC operated at 60 °C with a 0.005 M H₂SO₄ mobile phase flowing at 0.7 mL/min and detected with a UV detector at 210 nm.

2.4. Quality assurance and quality control

To ensure that the rig was appropriate for measurements of the UV-PCO system performance, various pre-qualification tests including an air leakage test, air velocity uniformity and stability tests, a concentration uniformity test and a no-filter test were conducted. The average leakage rate of 0.87% ± 0.07% did not exceed 1.0% of the test airflow rate of 240 m³/h (140 cfm), satisfying the ASHRAE standard 145.2–2016 [29]. No filter test was performed to check the adequacy of the overall duct, sampling, measurement, contaminant generator, leakage effect, and sink effect. The difference between the upstream and downstream ethanol concentrations was 0.39% ± 0.11%, less than 5% of the measured concentration [29]. The results of air velocity uniformity (coefficient of variance (CoV) = 1.7% ± 0.2%) and concentration uniformity (CoV = 3.3% ± 0.4%) quantitatively verified that the test rig was capable of providing reliable UV-PCO air cleaner efficiency measurements.

Method blanks were analyzed for each set of tests to ensure formaldehyde background of less than 1 ng/cartridge, and acetaldehyde background of 3 ng/cartridge. Duplicate DNPH samples were taken in some tests to check the stability and repeatability of by-products

Table 1

Summary statistics of experimental data and relationship between FA and independent variables (n = 36).

UV-PCO parameter	Mean ± SD	Min	Max	FA		FA	
				Pearson r	P	Spearman r	P
Inlet ethanol (ppb)	611.8 ± 387.3	242.0	2102.0	0.820	0.000	0.584	0.000
Outlet ethanol (ppb)	512.4 ± 352.2	135.0	1813.0	0.790	0.000	0.460	0.005
RH (%)	29.2 ± 14.8	9.2	59.7	-0.579	0.001	-0.581	0.000
Temperature (°C)	22.9 ± 1.6	20.8	25.7	0.099	0.564	0.229	0.179
Airflow (m ³ /h)	177.3 ± 30.3	125.2	262.5	-0.637	0.001	-0.636	0.001
Irradiance (W/m ²)	17.0 ± 3.0	7.5	21.7	0.843	0.000	0.571	0.003
Ozone (ppb)	938.8 ± 1258.7	6.6	5827.6	0.016	0.925	0.034	0.846
Formaldehyde (ppb)	25.5 ± 11.2	9.0	63.0	0.218	0.202	0.351	0.036
Acetaldehyde (ppb)	103.9 ± 71.3	12.8	350.3	0.988	0.000	0.977	0.000

Bold indicates that correlation is significant at the 0.05 level (2-tailed).

(CoV = 3.5%). The HPLC detection limit of formaldehyde and acetaldehyde was 0.03 ng/L.

2.5. Model development and statistical analysis

The model development was based on the sum of formaldehyde and acetaldehyde (FA) concentrations from the PCO experiments as an independent variable, while inlet and outlet ethanol values, RH, temperature, air flow rate, irradiance, and ozone concentration were designated as independent variables. Considering the mechanism of by-product formation is not clear, a linear model (Eq. (1)) and a non-linear regression model (Eq. (2)) were proposed and evaluated statistically. The most significant explanatory independent variables were selected using the results of the Pearson and Spearman tests.

$$FA = a + b(C_{inlet}) + c(C_{outlet}) + d(RH) + e(Temp) + f(AirFlow) + g(Irradiance) + h(Ozone) \quad (1)$$

$$FA = a(C_{inlet})^b(C_{outlet})^c(RH)^d(Temp)^e(AirFlow)^f(Irradiance)^g(Ozone)^h \quad (2)$$

Excel (Microsoft, 2016, Seattle, WA, USA) and SPSS Statistics v. 24 (SPSS Corporation, Chicago, IL, USA) were used for statistical analyses. The correlation analyses between each independent variable and the dependent variable were conducted in both Pearson and Spearman methods. Fitness and performance of the regression models were estimated by coefficients of correlation (R²), Durbin-Watson value, Kolmogorov-Smirnov Test, and plots of residuals versus predicted values.

2.6. Validation of developed models

The developed models were validated with (1) reference data [30] conducted in 2013, the same testing rig with lab-synthesized PCO filters (different substrates and photocatalysts) and (2) a small bench-top PCO reactor [31] challenged by ethanol (498–987 ppb) under the conditions of 0.5–2 L/min airflow rates, 10.2–50.1% RH, 7.5–15.7 W/m² UV irradiances. Plots of the predicted versus measured values were evaluated for two scenarios.

3. Results and discussion

3.1. UV-PCO test results

A total of 36 PCO-based HVAC air cleaning experiments was conducted in the year 2012. Table 1 lists the averages and ranges of each operational parameter (inlet and outlet ethanol concentration, RH, temperature, airflow, irradiance, and ozone concentration) and by-products (formaldehyde and acetaldehyde) in the PCO tests as well as Pearson and Spearman correlation coefficients. Ethanol with concentrations of 242–2102 ppb was introduced to the duct system under

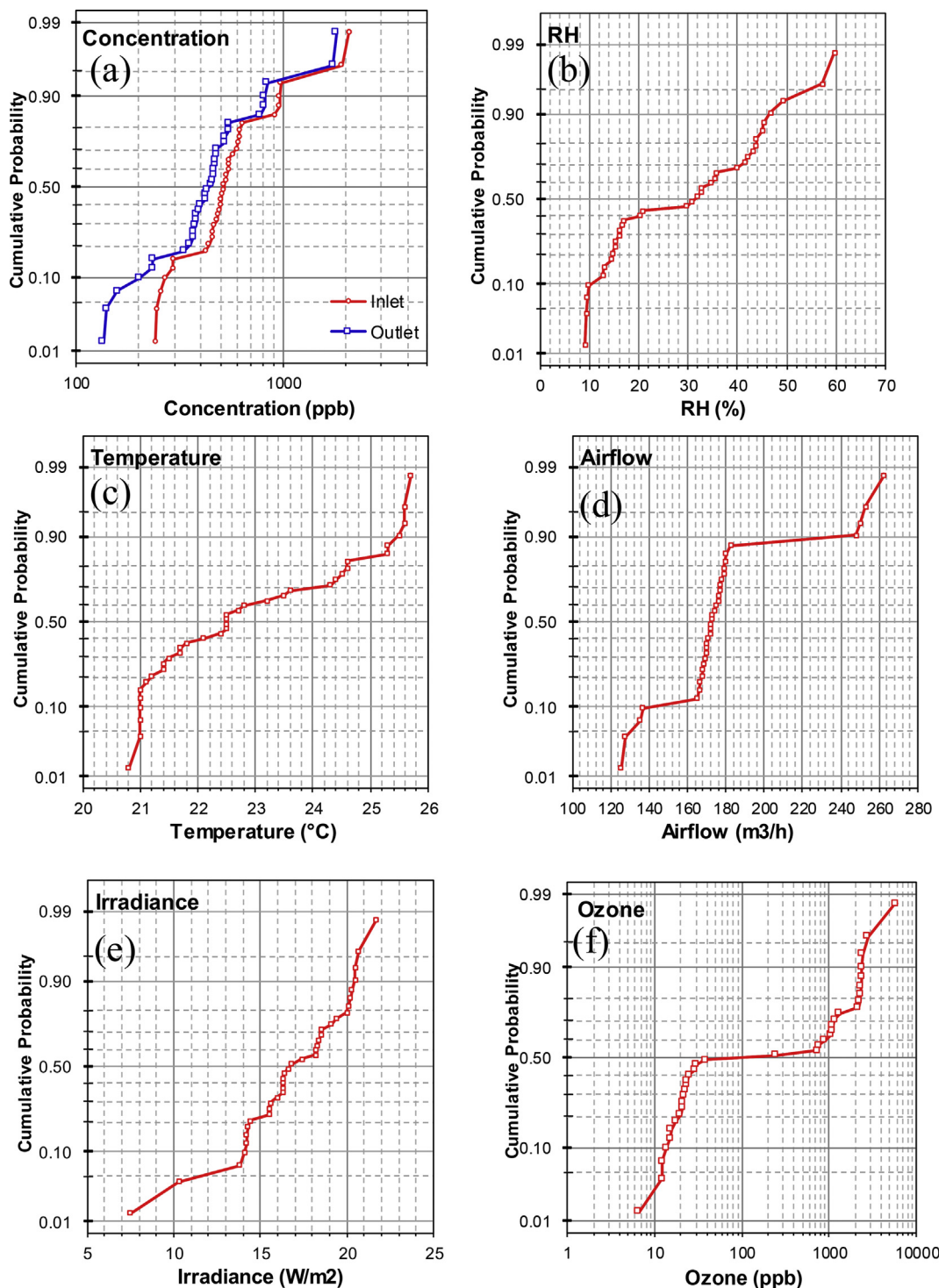


Fig. 2. Probability plots of (a) ethanol concentration, (b) RH, (c) temperature, (d) airflow, (e) irradiance, and (f) ozone in 36 UV-PCO tests.

the conditions of 9.2–59.7% RH, 125–262 m³/h airflow rates, 7.5–21.7 W/m² irradiance, and 6.6–5827.6 ppb ozone levels. Formaldehyde (25.5 ± 11.2 ppb) and acetaldehyde (103.9 ± 71.3 ppb) were 100% detected for all tests. Concentrations of ethanol and acetaldehyde were positively and significantly correlated with FA by two methods (Pearson and Spearman correlation coefficients ranged from 0.82 to 0.99 and 0.58 to 0.98, respectively). Notably, RH and airflow had significant inverse relationships with FA (−0.64 < r < −0.58). Probability plots of individual variable suggest that dependent variables were approximately normally distributed (Fig. 2). The results of the

Kolmogorov-Smirnov test (Table 2) further confirmed that all dependent variables followed the normal distribution at the significance level of 0.05.

It is noted that temperature was not a designed operational condition to check the PCO activity, so the narrow lab temperature range of 20.8–25.7 °C in this study was not sufficient to demonstrate a significant relationship with FA output. On the contrary, ozone was an intended parameter involved in the duct unit setting-up for exploration of the ozonation effect on PCO. However, both Pearson (r = 0.016) and Spearman (r = 0.034) analyses show a weak relationship between

Table 2
Kolmogorov-Smirnov test (n = 36).

		Inlet (ppb)	Outlet (ppb)	RH (%)	Temp (°C)	Flow (m ³ /h)	Irradiance (W/m ²)	Ozone (ppb)
Normal Parameters ^{a,b}	Mean	611.8	512.4	29.2	22.9	177.3	17.0	938.8
	Std. Dev.	392.8	357.2	15.0	1.6	30.7	3.0	1276.5
Most Extreme Differences	Absolute	0.305	0.290	0.184	0.144	0.327	0.105	0.260
	Positive	0.305	0.290	0.184	0.144	0.327	0.078	0.260
	Negative	-0.173	-0.145	-0.099	-0.113	-0.235	-0.105	-0.233
Test Statistic		0.305	0.290	0.184	0.144	0.327	0.105	0.260
Asymp. Sig. (2-tailed)		0.000 ^c	0.000 ^c	0.004 ^c	0.056 ^c	0.000 ^c	0.033 ^c	0.000 ^c

^a Test distribution is Normal.

^b Calculated from data.

^c Lilliefors Significance Correction.

Table 3
Pearson correlation coefficients of VOC concentrations and key operational parameters (n = 36).

	Inlet ethanol	Outlet ethanol	RH	Temp	Airflow	Irra-diance	Ozone	Formalde-hyde	Acetalde-hyde	FA
Inlet ethanol	1									
Outlet ethanol	0.996	1								
RH	-0.401	-0.362	1							
Temp	-0.116	-0.117	-0.135	1						
Airflow	-0.031	-0.013	0.024	0.027	1					
Irradiance	-0.064	-0.109	0.006	0.238	-0.159	1				
Ozone	-0.006	-0.052	0.032	-0.392	-0.155	0.527	1			
Formaldehyde	-0.017	-0.011	0.235	0.347	-0.259	0.346	0.010	1		
Acetaldehyde	0.841	0.810	-0.629	0.047	-0.608	0.745	0.015	0.066	1	
FA	0.820	0.790	-0.579	0.099	-0.637	0.843	0.016	0.218	0.988	1

Bold values are statistically significant (p < 0.05).

ozone and FA formation. More by-products, such as crotonaldehyde, acetone, propionaldehyde, and butyraldehyde, were detected in ozone-assisted PCO tests, indicating that the introduction of additional radicals by ozone leads to complexity of by-product formation. In addition, unlike acetaldehyde, the formaldehyde level was weakly related (r = 0.218–0.351) to FA generation. In order to deeply understand the mechanism of by-product formation in the PCO of ethanol, full bivariate correlation analysis was conducted and presented in Table 3, on the basis of which the parametric analysis and modeling work have been implemented.

3.2. Effect of ethanol concentration

Inlet and outlet concentrations of ethanol show strong relationships (r = 0.79–0.84) with acetaldehyde and FA levels (Table 3). Fig. 3 confirms that acetaldehyde and FA formation rose with increased inlet and outlet concentrations of ethanol. A high correlation (r = 0.988)

was obtained between FA and acetaldehyde, suggesting the rate of FA formation is close to that of acetaldehyde formation. This finding is in line with previous observations [3,8,30], indicating ethanol conversion to acetaldehyde is not the rate-limiting step in the PCO of ethanol. Muggli et al. (1998) [32] used temperature-programmed desorption technology to observe that approximately 15% of the ethanol monolayer rapidly converted to gaseous acetaldehyde. Hence, the higher availability of ethanol provides a bigger chance to form acetaldehyde if radicals are adequate. In addition, Fig. 3 and Table 3 show that formaldehyde formation was independent of inlet and outlet of ethanol concentration, implying that formaldehyde production underwent slow multiple-stage reactions during or after acetaldehyde formation, and multiple-stage reactions possibly generate some intermediates inhibiting formaldehyde conversion.

Here, it should be noted that although acetaldehyde and FA shows a positive correlation with ethanol outlet concentration, the ethanol outlet level is not a controllable parameter which is dependent on the

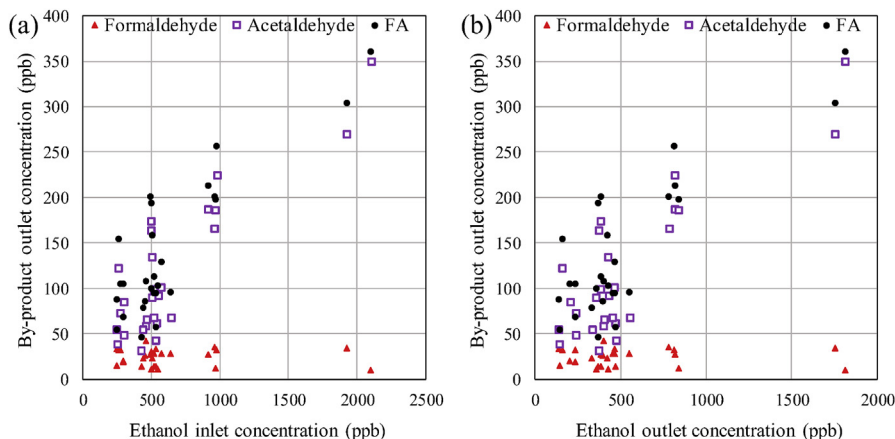


Fig. 3. Relationship between by-product concentrations and ethanol inlet (a) and outlet (b) concentrations.

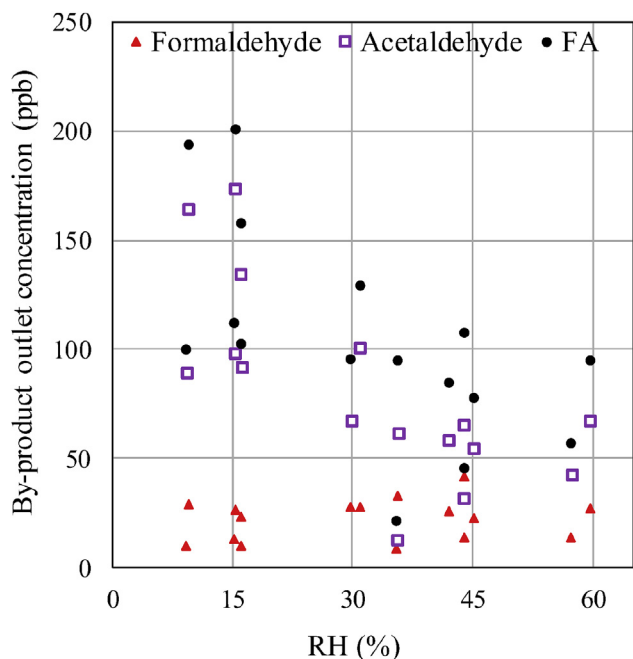


Fig. 4. Relationship between by-product concentrations and RH.

PCO filter performance. The involvement of ethanol outlet concentration in the modeling development is to account for the effect of the PCO efficiency on the by-product formation. Therefore, the positive correlation does not mean that high ethanol output helps the generation of acetaldehyde or FA. The actual contribution of ethanol outlet concentration needs to be determined by a regression method.

3.3. Effect of RH

A significant influence of RH on the PCO degradation process and the by-product generation was observed and discussed by many researchers [1,2,8,18,19,33,34]. It has been concluded that lower water vapor helps to obtain higher decomposition efficiency partly due to less competitive adsorption of water vapor and target VOCs on the photocatalysts, and partly due to lower electron-hole recombination. Shayegan et al. (2018) found, after surface fluorination, the modified TiO₂ with less hydrophilic property increased its VOC adsorption capacity. However, the effect of RH on by-product formation was difficult to be characterized due to large differences in the experimental conditions and the complexity of by-products. Our test results (Fig. 4) agree with Mo et al. (2013) [19]’s finding that the maximum efficiency does not always lead to minimal by-products. Less RH is beneficial to oxidize ethanol, which does not ensure the PCO process is complete oxidation. It is not surprising to see the trend of more acetaldehyde and FA generation at low RH levels (Fig. 4). Moreover, formaldehyde is still not affected by RH. These phenomena can be explained by the reasonable assumption that some chemically adsorbed intermediates existing between acetaldehyde and formaldehyde inhibited acetaldehyde to be further oxidized.

3.4. Effect of irradiance

Previous researchers found a first-order or half-order kinetic function correlation between the PCO reaction rate and the light intensity [8,35,36]. It is interesting to find that in this study all tested by-products (formaldehyde, acetaldehyde, and FA) increased with an increase of the irradiance from 7.5 to 20.5 W/m² as shown in Fig. 5. Similar observations were made by Vincent et al. (2009) [37] for the PCO of 1-propanol. Pearson correlation matrix (Table 3) indicated significant

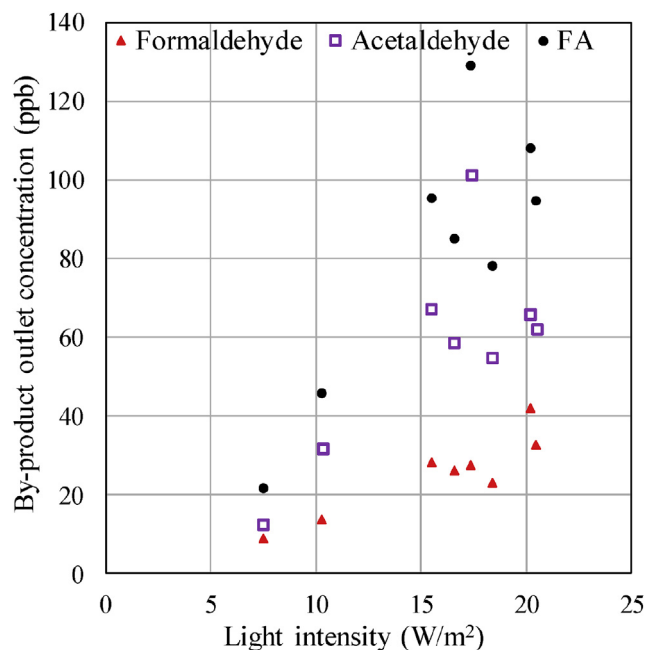


Fig. 5. Relationship between by-product concentrations and light intensity.

relationships of irradiance with formaldehyde ($r = 0.346$), acetaldehyde ($r = 0.745$), and FA ($r = 0.843$). Especially, the increasing trend of formaldehyde production with irradiance indicates the higher energy provided helps acetaldehyde or other chemisorbed intermediates (possible acids) convert to formaldehyde. Hence, limited UV irradiance exposure is the rate-limiting operational parameter for mineralization in the present study.

3.5. Effect of airflow

The effect of air flow on formaldehyde, acetaldehyde and FA outlet concentrations were investigated in the range of 125.2 m³/h (residence time (RT) \approx 25 m s) to 262.5 m³/h (RT \approx 12 m s). From Fig. 6, we can observe that FA and acetaldehyde outlet concentrations decreased from

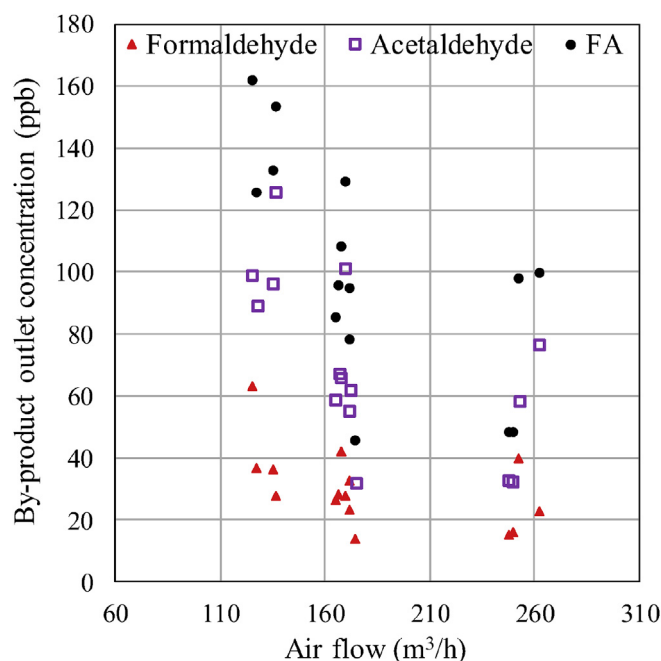


Fig. 6. Relationship between by-product concentrations and airflow.

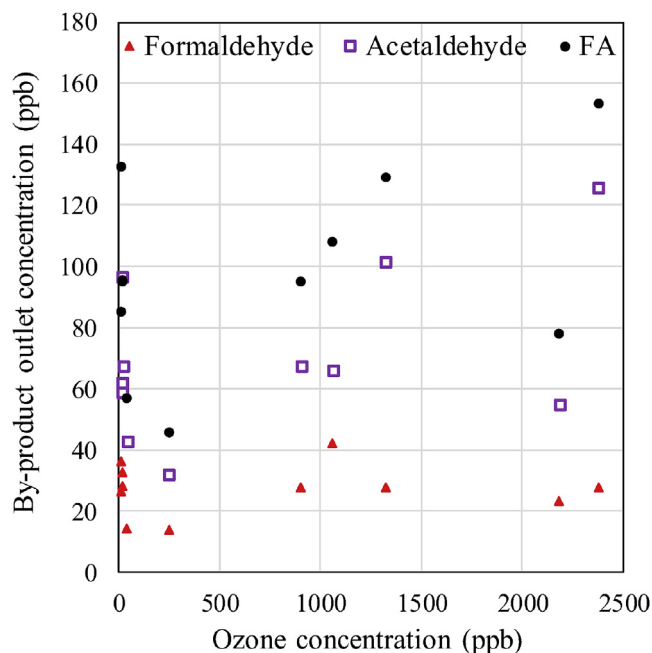


Fig. 7. Relationship between by-product concentrations and ozone level.

132.8–162.1 ppb to 48.2–99.6 ppb and from 96.4–125.8 ppb to 32.4–76.6 ppb, respectively, as the airflow was enhanced. This trend agrees with Vincent et al.'s [37] observation that by-product concentrations increased with the increase of the contact time under UV exposure. The previous study found PCO reaction rates were nearly constant as airflow rates increased from 0.2 to 2 L/min [9]. Compared with the low airflow case, our study suggests that the surface photochemical reaction rate, rather than the mass transfer between gas and solid phases in the reactor, was the controlling step. Hence, dilution is the dominant reason to reduce the acetaldehyde and FA concentrations as the airflow rates increased. In addition, an insignificant correlation ($r = 0.218$) between formaldehyde and FA further indicates that the mass transfer was not the limiting process (high flow had no contribution to formaldehyde production).

3.6. Effect of ozone concentration

Ozone showed no significant contribution on formaldehyde ($r = 0.010$), acetaldehyde ($r = 0.015$), and FA ($r = 0.016$) production when ozone levels arose from 12.4 ppb to 2377.4 ppb (Fig. 7). The previous study found the ozone-assisted UV-PCO could improve the removal efficiency due to the enhancement of electron capture. From the by-product perspective, more hydroxyl radicals introduced by ozone did not favor the specific by-product formation, but it led to trace amounts of other by-product production, such as acetone, crotonaldehyde, and propionaldehyde.

3.7. By-product modeling

Mathematical models were developed using linear and nonlinear regression approaches. Inlet and outlet concentration, RH, airflow, and irradiance were selected as final independent variables on the basis of the above-mentioned Pearson and Spearman analyses (Table 1). Eqs (1) and (2) were optimized to Eqs (3) and (4), which can predict FA or acetaldehyde formation. The concentration is expressed in ppb, RH in % by 100, airflow in m^3/h , and irradiance in W/m^2 .

$$\text{FA (acetaldehyde)} = a + b(C_{\text{inlet}}) + c(C_{\text{outlet}}) + d(\text{RH}) + e(\text{AirFlow}) + f(\text{Irradiance}) \quad (3)$$

Table 4

Results of statistical linear and non-linear regression for FA and acetaldehyde.

	FA		Acetaldehyde	
	Linear	Non-linear	Linear	Non-linear
Coefficient of correlation (R)	0.897	0.895	0.922	0.921
R ²	0.804	0.801	0.850	0.848
Std. Error of the estimate	35.326	0.341	30.200	0.377
Durbin-Watson	2.085	2.247	1.961	2.044
F value	24.629	14.313	34.094	16.875
ANOVA sig.	0.000	0.000	0.000	0.000
Statistical coefficients				
a	92.101	138.356	79.987	173.388
b	0.374	0.951	0.453	0.876
c	-0.262	-0.347	-0.351	-0.245
d	-1.175	-0.315	-1.297	-0.481
e	-0.333	-0.728	-0.244	-0.736
f	2.134	0.265	0.475	0.245

$$\text{FA (acetaldehyde)} = a(C_{\text{inlet}})^b(C_{\text{outlet}})^c(\text{RH})^d(\text{AirFlow})^e(\text{Irradiance})^f \quad (4)$$

ANOVA test results of the statistical coefficients, coefficients of correlation, the standard errors, Durbin-Watson, and F-value for the proposed models are presented in Table 4. In terms of coefficient of correlation (R), it appears that the linear and nonlinear models are similar for both FA and acetaldehyde prediction. In addition, due to no interference by formaldehyde, the linear ($R^2 = 0.850$) and nonlinear ($R^2 = 0.848$) models for acetaldehyde prediction are better than the ones ($R^2 \approx 0.8$) for FA prediction. Durbin-Watson values of 1.961–2.247 are within the range of 1.5–2.5, statistically confirming the goodness fit of developed models [38]. Moreover, for the proposed FA and acetaldehyde models, the mean values of residuals are zero, and Fig. 8 shows residuals for all cases are evenly distributed around the zero baselines, indicating variables involved in the models are adequate to describe the FA and acetaldehyde formation. All statistical coefficients for both linear and nonlinear models show the same trends: inlet concentration and light intensity have a positive contribution to FA and acetaldehyde generation; while outlet concentration, RH, and airflow inversely related to FA and acetaldehyde formation.

3.8. Model validation

Fig. 9 (a)-(b) presents the comparison between predicted and observed values for FA models at two air flow modes. The linear ($R^2 = 0.83$) and nonlinear ($R^2 = 0.84$) FA models are in agreement with results of previous study [30] employing the same duct system with different PCO filters, indicating both linear and nonlinear techniques are effective in predicting FA levels in a PCO system at a high airflow (160–180 m^3/h) mode with diverse PCO filters. However, as shown in Fig. 9 (b), the linear FA model ($R^2 = 0.74$) is superior to the nonlinear FA model ($R^2 = 0.06$) for a PCO system under a slow airflow mode (0.5–2 L/min), implying that linear modeling approach has a more precise prediction ability of FA concentrations at a wide range of airflow modes. Fig. 9 (c)-(d) shows the acetaldehyde can be estimated more precisely than FA due to different formation mechanisms of acetaldehyde and formaldehyde in the PCO of ethanol. Similarly, the linear acetaldehyde model ($R^2 = 0.72$) is more accurate than the nonlinear one ($R^2 = 0.17$) at low airflow applications. Therefore, the multiple nonlinear regression model is sensitive to the airflow, and the linear model is more useful to predict by-products in wide applications.

3.9. Reaction pathway

In our study, we detected only formaldehyde and acetaldehyde as the major VOCs in the gas phase. No detection of other gaseous compounds, such as acids, by HPLC in the non-ozone involved UV-PCO

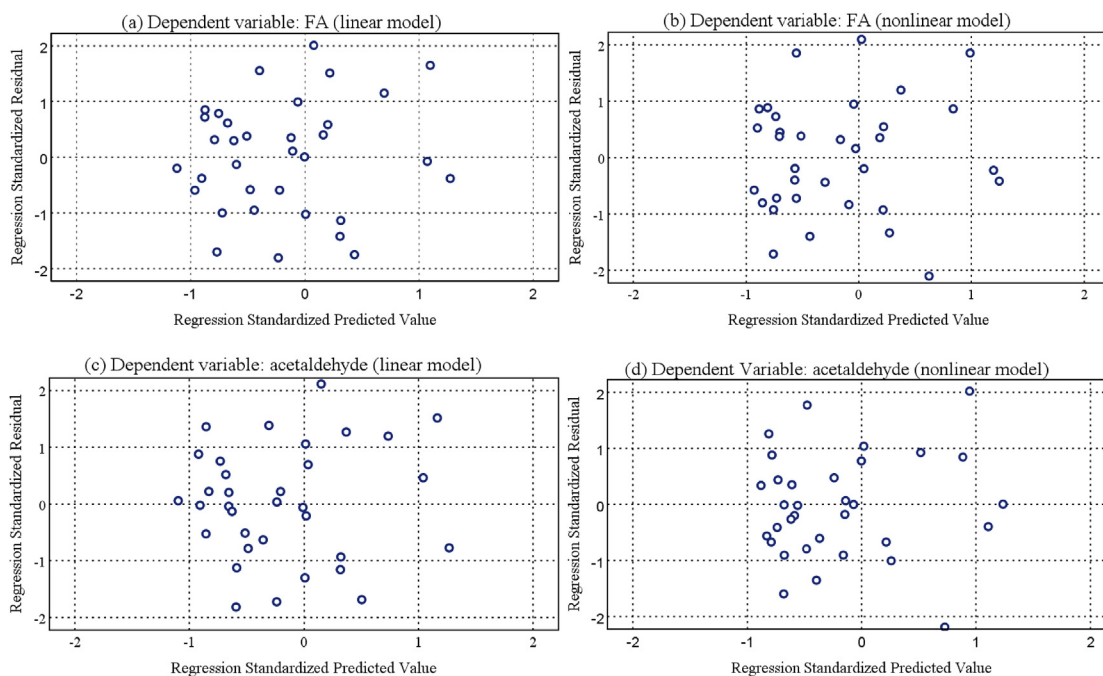


Fig. 8. Plots of residuals versus predicted values for (a) FA linear model, (b) FA nonlinear model, (c) acetaldehyde linear model, and (d) acetaldehyde nonlinear model.

tests. Detectable acids (e.g. formic acid and acetaldehyde acid) attached to substrates were reported by some researchers using surface extraction technologies [30,39,40]. The absence of detectable acids in the gas

phase in this study further confirmed that the strong adsorptive properties of acids during the PCO process. Nimlos et al. investigated the primary products from PCO of ethanol, acetaldehyde, acetic acid, and

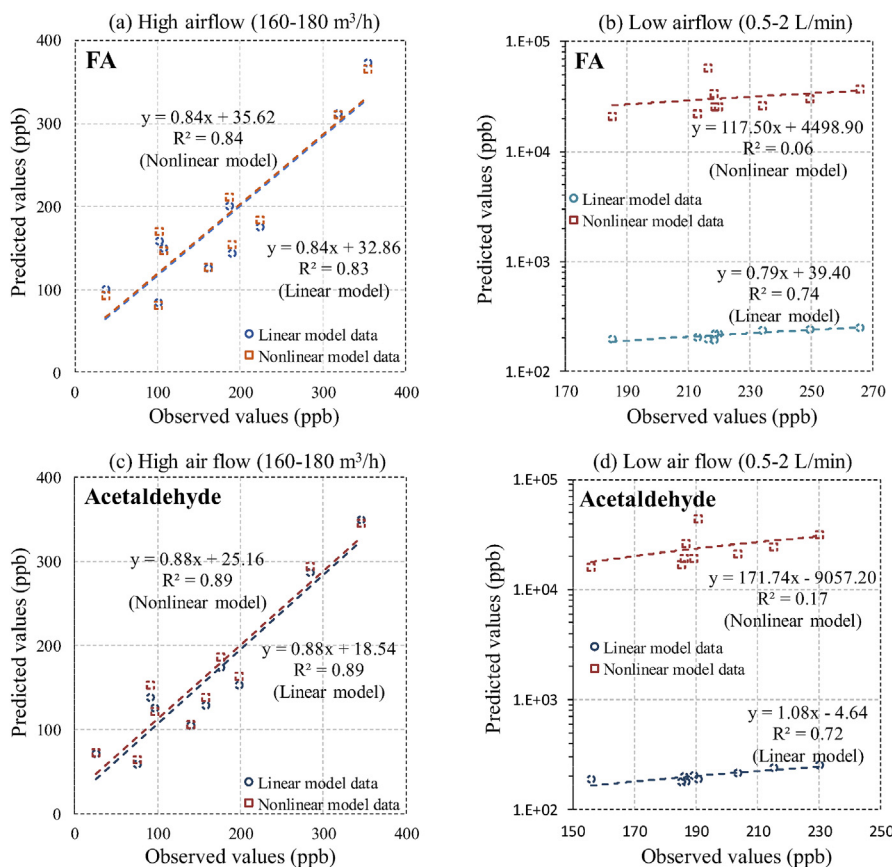


Fig. 9. Comparison between predicted and observed values for (a) FA at high airflow rates, (b) FA at low airflow rates, (c) acetaldehyde at high airflow rates, and (d) acetaldehyde at low airflow rates.

- photocatalytic air cleaners: efficiencies and by-product generation, *Environ. Sci. Pollut. Control Ser.* 23 (2016) 7482–7493.
- [5] Z. Shayegan, C. Lee, F. Haghighat, TiO₂ photocatalyst for removal of volatile organic compounds in gas phase - a review, *Chem. Eng. J.* 334 (2018) 2408–2439.
- [6] L. Zhong, F. Haghighat, Photocatalytic air cleaners and materials technologies - abilities and limitations, *Build. Environ.* 91 (2015) 191–203.
- [7] L. Zhong, C. Lee, F. Haghighat, A. Bahloul, Deactivation and ultraviolet C-induced regeneration of photocatalytic oxidation air filters, *Sci. Technol. Built. Environ.* 22 (2016) 576–585.
- [8] L. Zhong, F. Haghighat, C. Lee, N. Lakdawala, Performance of ultraviolet photocatalytic oxidation for indoor air applications: systematic experimental evaluation, *J. Hazard Mater.* 261 (2013) 130–138.
- [9] L. Zhong, J.J. Brancho, S. Batterman, B.M. Bartlett, C. Godwin, Experimental and modeling study of visible light responsive photocatalytic oxidation (PCO) materials for toluene degradation, *Appl. Catal. B Environ.* 216 (2017) 122–132.
- [10] K. Nakahara, T. Yamaguchi, E. Lim, K. Ito, Computational fluid dynamics modeling and parameterization of the visible light photocatalytic oxidation process of toluene for indoor building material, *Sustain. Cities Soc.* 35 (2017) 298–308.
- [11] Y. Deng, Developing a Langmuir-type excitation equilibrium equation to describe the effect of light intensity on the kinetics of the photocatalytic oxidation, *Chem. Eng. J.* 337 (2018) 220–227.
- [12] J. Roegiers, J. van Walsem, S. Denys, CFD- and radiation field modeling of a gas phase photocatalytic multi-tube reactor, *Chem. Eng. J.* 338 (2018) 287–299.
- [13] M. Lin, C. Jwo, H. Ho, L. Chen, Using box modeling to determine photodegradation coefficients describing the removal of gaseous formaldehyde from indoor air, *Aerosol Air Qual. Res.* 17 (2017) 330–339.
- [14] J. van Walsem, S.W. Verbruggen, B. Modde, S. Lenaerts, S. Denys, CFD investigation of a multi-tube photocatalytic reactor in non-steady-state conditions, *Chem. Eng. J.* 304 (2016) 808–816.
- [15] R.S. Pelzers, Q.L. Yu, R.A. Mangkuto, Radiation modeling of a photo-reactor using a backward ray-tracing method: an insight into indoor photocatalytic oxidation, *Environ. Sci. Pollut. Control Ser.* 21 (2014) 11142–11154.
- [16] X. Wang, X. Tan, T. Yu, Modeling of formaldehyde photocatalytic degradation in a Honeycomb monolith reactor using computational fluid dynamics, *Ind. Eng. Chem. Res.* 53 (2014) 18402–18410.
- [17] L. Zhong, F. Haghighat, C. Lee, Ultraviolet photocatalytic oxidation for indoor environment applications: experimental validation of the model, *Build. Environ.* 62 (2013) 155–166.
- [18] J. Mo, Y. Zhang, Q. Xu, Y. Zhu, J.J. Lamson, R. Zhao, Determination and risk assessment of by-products resulting from photocatalytic oxidation of toluene, *Appl. Catal. B Environ.* 89 (2009) 570–576.
- [19] J. Mo, Y. Zhang, Q. Xu, Effect of water vapor on the by-products and decomposition rate of ppb-level toluene by photocatalytic oxidation, *Appl. Catal. B Environ.* 132 (2013) 212–218.
- [20] D.S. Selishchev, N.S. Kolobov, A.A. Pershin, D.V. Kozlov, TiO₂ mediated photocatalytic oxidation of volatile organic compounds: formation of CO as a harmful by-product, *Appl. Catal. B Environ.* 200 (2017) 503–513.
- [21] I. Dhada, M. Sharma, P.K. Nagar, Quantification and human health risk assessment of by-products of photo catalytic oxidation of ethylbenzene, xylene and toluene in indoor air of analytical laboratories, *J. Hazard Mater.* 316 (2016) 1–10.
- [22] O. d'Hennezel, P. Pichat, D.F. Ollis, Benzene and toluene gas-phase photocatalytic degradation over H₂O and HCL pretreated TiO₂: by-products and mechanisms, *J. Photochem. Photobiol. Chem.* 118 (1998) 197–204.
- [23] C.P. Huang, D.H. Chen, K.Y. Li, Photocatalytic oxidation of butyraldehyde over titania in air: by-product identification and reaction pathways, *Chem. Eng. Commun.* 190 (2003) 373–392.
- [24] J. Jeong, K. Sekiguchi, W. Lee, K. Sakamoto, Photodegradation of gaseous volatile organic compounds (VOCs) using TiO₂ photoirradiated by an ozone-producing UV lamp: decomposition characteristics, identification of by-products and water-soluble organic intermediates, *J. Photochem. Photobiol. Chem.* 169 (2005) 279–287.
- [25] H.M. Liu, X.J. Ye, Z.W. Lian, Y.G. Wen, W.F. Shangguan, Experimental study of photocatalytic oxidation of formaldehyde and its by-products, *Res. Chem. Intermed.* 32 (2006) 9–16.
- [26] C.P. Chang, J.N. Chen, M.C. Lu, Characteristics of photocatalytic oxidation of gaseous 2-propanol using thin-film TiO₂ photocatalyst, *J. Chem. Technol. Biotechnol.* 79 (2004) 1293–1300.
- [27] H. Dylla, S. Asadi, M. Hassan, L.N. Mohammad, Evaluating photocatalytic asphalt pavement effectiveness in real-world environments through developing models: a statistical and kinetic study, *Road Mater. Pavement Des.* 14 (2013) 92–105.
- [28] H. Ibrahim, H. de Lasa, Kinetic modeling of the photocatalytic degradation of airborne pollutants, *AIChE J.* 50 (2004) 1017–1027.
- [29] ASHRAE, ASHRAE 145.2 Laboratory Test Method for Assessing the Performance of Gas-phase Air-cleaning Systems: Air-cleaning Devices, (2016).
- [30] A. Aghighi, F. Haghighat, L. Zhong, C. Lee, Evaluation of ultraviolet-photocatalytic oxidation of light alcohols at sub-parts per million concentrations, *Sci. Technol. Built. Environ.* 21 (2015) 160–171.
- [31] L. Zhong, J.J. Brancho, S. Batterman, B.M. Bartlett, C. Godwin, Experimental and modeling study of visible light responsive photocatalytic oxidation (PCO) materials for toluene degradation, *Appl. Catal. B Environ.* 216 (2017) 122–132.
- [32] D.S. Muggli, J.T. McCue, J.L. Falconer, Mechanism of the photocatalytic oxidation of ethanol on TiO₂, *J. Catal.* 173 (1998) 470–483.
- [33] W. Abou Saoud, A.A. Assadi, M. Guiza, A. Bouzaza, W. Aboussaoud, I. Soutrel, et al., Abatement of ammonia and butyraldehyde under non-thermal plasma and photocatalysis: oxidation processes for the removal of mixture pollutants at pilot scale, *Chem. Eng. J.* 344 (2018) 165–172.
- [34] Z. Shayegan, F. Haghighat, C. Lee, A. Bahloul, M. Huard, Effect of surface fluorination of P25-TiO₂ on adsorption of indoor environment volatile organic compounds, *Chem. Eng. J.* 346 (2018) 578–589.
- [35] T.N. OBEE, R.T. BROWN, TiO₂ photocatalysis for indoor air applications - effects of humidity and trace contaminant levels on the oxidation rates of formaldehyde, toluene, and 1,3-butadiene, *Environ. Sci. Technol.* 29 (1995) 1223–1231.
- [36] L. Zhong, F. Haghighat, P. Blondeau, J. Kozinski, Modeling and physical interpretation of photocatalytic oxidation efficiency in indoor air applications, *Build. Environ.* 45 (2010) 2689–2697.
- [37] G. Vincent, P.M. Marquaire, O. Zahraa, Photocatalytic degradation of gaseous 1-propanol using an annular reactor: kinetic modelling and pathways, *J. Hazard Mater.* 161 (2009) 1173–1181.
- [38] M. Kumari, S.K. Gupta, Modeling of trihalomethanes (THMs) in drinking water supplies: a case study of eastern part of India, *Environ. Sci. Pollut. Control Ser.* 22 (2015) 12615–12623.
- [39] J. Shang, Y.G. Du, Z.L. Xu, Photocatalytic oxidation of heptane in the gas-phase over TiO₂, *Chemosphere* 46 (2002) 93–99.
- [40] M.R. Nimlos, E.J. Wolfrum, M.L. Brewer, J.A. Fennell, G. Binter, Gas-phase heterogeneous photocatalytic oxidation of ethanol: pathways and kinetic modeling, *Environ. Sci. Technol.* 30 (1996) 3102–3110.